Contrib Mineral Petrol (2016) 171:6
DOI 10.1007/s00410-015-1213-9

ORIGINAL PAPER

Clinopyroxene in postshield Haleakala ankaramite: 2. Texture, compositional zoning and supersaturation in the magma

Benoit Welsch[1] · Julia Hammer[1] · Alain Baronnet[2] · Samantha Jacob[1] · Eric Hellebrand[1] · John Sinton[1]

Received: 14 July 2015 / Accepted: 20 November 2015

Abstract We investigated the external morphologies and internal compositional zoning patterns of clinopyroxene phenocrysts in an ankaramite of Haleakala volcano (Hawaii) to constrain magma crystallization conditions in the volcano's postshield stage. The phenocrysts are characterized by euhedral faceted morphologies and crystallographically coherent subcrystals. Quantitative EPMA and X-ray element mapping reveal two domains within the crystals: porous, Si–Mg–Ca–Cr-rich zones associated with the forms {100}, {010} and {110}, and nonporous, Al–Ti–Na-rich zones associated with the forms {−111}. The chemical variations, internal porosity and parallel subcrystals are consistent with nonconcentric crystal growth at varying degrees of supersaturation. We infer that initial growth occurred in a diffusion-limited regime to produce dendritic crystals; subsequent growth was markedly slower, with lesser supersaturation allowing dendrites to infill and produce polyhedral external morphologies. This sequence promoted the evolution of crystals from an hourglass shape with dominant {−111} forms, to sector-zoned euhedral crystals in which elements were partitioned according to: $(Al + Ti + Na)_{\{-111\}} = (Si + Mg + Cr + Ca)_{\{110\},\{100\},\{010\}}$. Infilling of dendritic crystals occurred to a greater extent on faster-growing sectors and was interrupted by the eruption, resulting in porosity of the slower-growing {hk0} sectors. Outermost Na-poor rims formed on all sectors due to slower growth rate under interface-limited conditions. Paradoxically, high levels of supersaturation producing large crystals of clinopyroxene (and olivine) are indicated in the volcano's deep-seated reservoir and lower degrees of supersaturation characterize syneruptive crystal growth. The presence of vapor bubbles within the melt-filled crystal embayments and inclusions suggests rapid clinopyroxene growth caused volatile saturation and reservoir pressurization, leading to eruption of the ankaramite.

Keywords Clinopyroxene · Sector zoning · Dendrite · Magma chamber

Introduction

The profound effect of supersaturation on the morphology and composition of crystals forming in magmas has long been appreciated from experimental work (e.g., Corrigan 1982; Lofgren and Donaldson 1975). The degree of supersaturation, or thermodynamic effective undercooling ($-\Delta T$) imposed by either varying environmental conditions or compositional changes in the liquid, controls the rates at which crystals nucleate and grow. In relation to the rate at which elements diffuse in the liquid, the growth rate in turn determines whether minor and trace elements are partitioned to the crystal in proportion to their liquid abundances, or whether uptake is far from equilibrium. The growth rate also determines whether a crystal develops

Communicated by Gordon Moore.

Electronic supplementary material The online version of this article (doi:10.1007/s00410-015-1213-9) contains supplementary material, which is available to authorized users.

✉ Benoit Welsch
bwelsch@hawaii.edu

[1] Department of Geology and Geophysics, University of Hawaii, 1680 East-West Road, Honolulu, HI, USA

[2] CINaM-CNRS, UPR 3118, Université Aix-Marseille, Campus Luminy, case 913, 13288 Marseilles Cedex 9, France

Published online: 15 December 2015

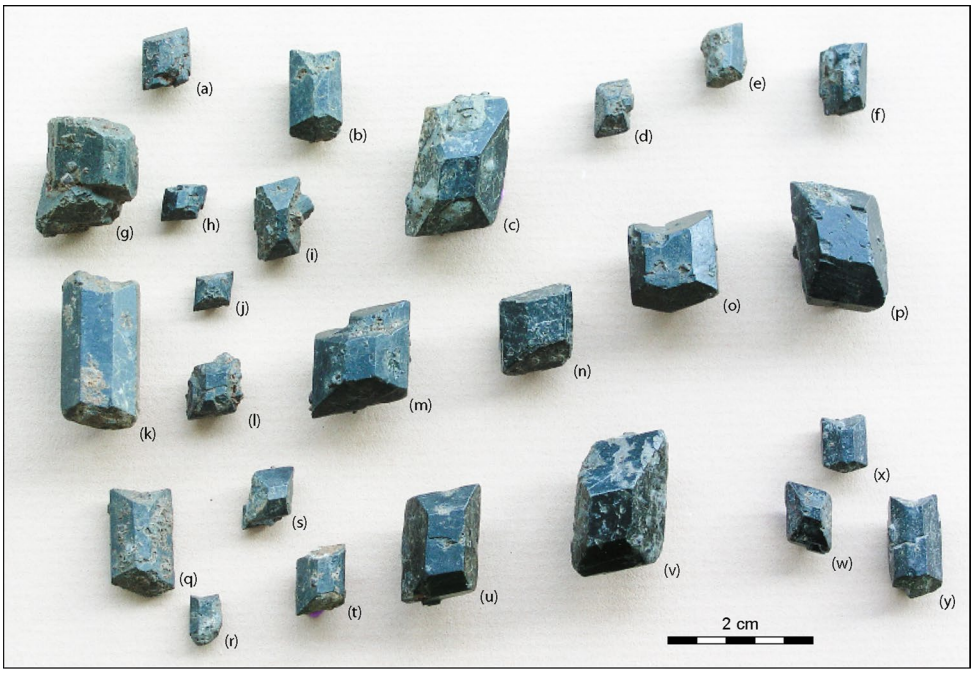

Fig. 1 Clinopyroxene phenocrysts weathered out from the Ka/Qkuls ankaramite of Haleakala volcano (Hawaii). The crystals are shown with their faces (010) or (0−10) oriented vertically. The *gray-brown* areas on the faces are residues of the ankaramite mesostasis. Mineralogical data reported in Fig. 2 indicate that crystals (*b*), (*k*), (*o*), (*q*), (*r*), (*x*) and (*y*) are twins {100}, and crystal (*g*) and (*i*) are twins {122}. Importantly, the parallel subcrystals observed in crystals (*d*), (*h*), (*l*), (*m*), (*p*), (*s*), (*u*) and (*w*) do not correspond to any twin laws

planar faces or branched protrusions, hoppers and scalloped embayments. Thus, the supersaturation, or magnitude of the chemical driving force for magma solidification, exerts a first-order control on both the textures of igneous rocks and the compositional evolution of coexisting minerals and liquids. Growth of crystals that are in chemical equilibrium with the surrounding liquid is, of course, impossible because the thermodynamic driving force for solidification is zero. However, if crystals grow at small driving force, near equilibrium, classical growth theory predicts the development of sharp vertices between planar faces (Hartman and Perdok 1955a, b, c). When the rate of growth unit attachment is very nearly balanced by the rate of detachment, convex euhedral crystals composed of low-energy, slow-advancing faces dominate the morphology and minimize the overall crystal–liquid interfacial free energy, ideally producing a compositionally homogeneous polyhedral crystal (i.e., Wulff crystal; Herring 1951). In contrast, rapid growth at higher supersaturation increases the frequency of high-energy defects such as screw dislocations and plateau steps, nonstoichiometric (impurity) cations, growth twins, embayments and protuberances. As might be expected, an evolution from one growth regime to another may result in a compound morphology and/or compositional heterogeneity inherited from growth at both low and high supersaturations. For example, olivine crystals grown at initially low supersaturation develop euhedral morphologies, and subsequent growth at higher supersaturation causes the flat faces to develop dendritic protrusions (Faure et al. 2007; Ni et al. 2014).

Euhedral crystals of clinopyroxene in ankaramite lavas and pyroclastic materials erupted during the postshield stage of Haleakala volcano, Hawaii, figure prominently in formative studies of the volcano (Cross 1915; Daly 1911; Washington and Mervin 1922) as hallmarks of alkalic basalt magmatism and as exemplars of the monoclinic 2/m crystal point group. Their morphologic near-perfection (Fig. 1) coupled with relatively restricted major element compositional variation (Fodor et al. 1975) supports the interpretation that these are slowly grown crystals, incubated in the subvolcanic magma reservoir over long timescales at conditions at low supersaturation (Stearns and Macdonald 1942). The assumption of chemical equilibrium underpins applications of clinopyroxene–melt thermobarometry to constrain the temperature and pressure in the reservoir prior to magma ascent (Chatterjee et al. 2005). The present study incorporates evaluation of the external morphologies of fortuitously isolated, macroscopically euhedral clinopyroxene crystals in hand specimen and secondary electron imaging, with spatially contextualized compositional analysis of crystal interiors. This study takes as a starting point the inference that euhedral clinopyroxene crystals from an ankaramite flow at the summit of Haleakala represent formation at low supersaturation, and examines whether the external morphologies and internal compositional variations conform to the predictions consistent with this hypothesis. A companion study (Hammer et al. this issue) investigates the application of clinopyroxene–liquid thermobarometry to these crystals.

Methods

Orientation indexing

Because the dominant forms (i.e., the sets of symmetrically equivalent faces) in the Haleakala clinopyroxene are limited in number (Fig. 1; Washington and Mervin 1922), crystal orientation indexing is accomplished by comparing the interfacial angles in thin section with those calculated using the appropriate lattice parameters and constraints afforded by the point group symmetry (Clark et al. 1969; Steno 1669). The 3D shape of the ideal clinopyroxene polyhedron, forms, interfacial angles, partings, cleavages, twinning laws and sector zoning of augite were computed and drawn using SHAPE 7.2 software (Dowty 1980, 1987; Fig. 2). Knowledge of common clinopyroxene twin laws (Rosenbusch 1888), partings and cleavages (Deer 1997) provide additional constraints in determining whether an external surface is a growth face, and whether nearby crystals are related crystallographically, e.g., as growth protrusions or twins, even if they are not contiguous within the section plane.

Imaging crystals in 3D

The sampling locality, petrography and geologic context are detailed in Hammer et al. (this issue). Fragments from two lava samples and three loose crystals of clinopyroxene were mounted in epoxy and prepared as polished thin sections for optical microscopic examination. The orientation and indexation of clinopyroxene crystal faces were determined by measuring the angles between the observed faces, taking into account lens distortion at the periphery of images. The mesostasis-free clinopyroxene crystals were imaged with secondary electrons using the JEOL JSM-6320F scanning electron microscope at CINaM-CNRS of the University of Aix-Marseille (France), equipped with a cold field-emission source and tuned at 3 keV. The crystals were glued onto a sticky graphite tape and coated with an evaporated 20-nm-thick amorphous C layer for electron conduction. Several clinopyroxene crystals were also photographed with stereomicroscope in the three principal crystallographic directions.

Electron probe X-ray intensity mapping

Ten sets of five elemental maps were acquired on nine different crystals of clinopyroxene, including two acquisitions on a mesostasis-free crystal, Augite3 (Fig. SM2). The maps were obtained with the JEOL Hyperprobe JXA-8500F electron microprobe of the University of Hawaii—Manoa (USA). The beam was tuned for scanning at 15 kV, 50–300 nA, with a probe diameter of 1–2 μm dwelled at 20–30 ms. Each map was acquired in 4–8 h with a step size of 3–8 μm at resolutions ranging between 600 and 1024 pixels in *X* by 900–1024 pixels in *Y*. The distribution of elements was measured using five diffracting crystals among six at a time, including two TAPs (for Al and Mg), one LIFH (for Cr), one TAPH (for Na), one PETJ (for Si, Ti or Ca) and one LIF (for V).

Two X-ray maps of two different olivine phenocrysts were acquired with the same microprobe using the methods given in Milman-Barris et al. (2008) and Welsch et al. (2014). The beam was tuned at 15 kV and 300 nA, with a probe diameter of 2 μm and a dwell time of 100 ms. The maps were acquired in 7 and 11 h, respectively, with a step size of 3 and 4 μm at resolutions of 600 and 700 pixels in *X* by 850 pixels in *Y*. The distribution of elements was measured using two PETHs (for P), one TAP (for Al), one LIF (for Cr) and one PETJ (for Ti).

Results

Clinopyroxene phenocrysts

The phenocrysts occur as both isolated crystals (Fig. 3a, b, f) and groups of adjacent units (Figs. 3e, 4). Most of the single crystals and crystal units have a polyhedral, equant habit (for example axis length ratios *a*:*b*:*c*–1.03:1:1.01 in Fig. 4a) and are characterized by a consistent set of dominant crystal forms {−111}, {110}, {100} and {010} (Figs. 3a, b, f, 4a, b, d, 5, 6). Within a given crystal or unit, the symmetrically equivalent faces are commonly slightly different in size: for example, the face (100) is larger than the face (−100) in Fig. 4a, and the face (010) is larger than the face (0−10) in crystal Ka01-26MCK of Fig. 6. Whereas the surfaces of the {hk0} forms, parallel to the *c*-axis, are macroscopically and microscopically smooth, the surfaces of the sole *c*-crossing {hk1} form, {−111}, are often irregular. These faces are microscopically rough due to abundant plateau steps, embayments and deep cavities (Figs. 3, 4). This is consistent with the occurrence of strong periodic bond chains along *c*-axis, which tend to stabilize the flatness of concordant forms {hk0} over the discordant forms {−111} (Hartman and Perdok 1955a, b, c).

Within contiguous groups of crystals, individual units typically share the same optical orientation (i.e., exhibit the same optical retardation and simultaneous extinction, Fig. 5). In the vast majority of cases where adjacent crystals exhibit one or more parallel faces, regardless of size, all the crystal units of a group are crystallographically aligned and exhibit several faces in contact with the mesostasis. Such instances are identified as buds in Figs. 4 and 5a, b, d, e, f. The units of a group are occasionally

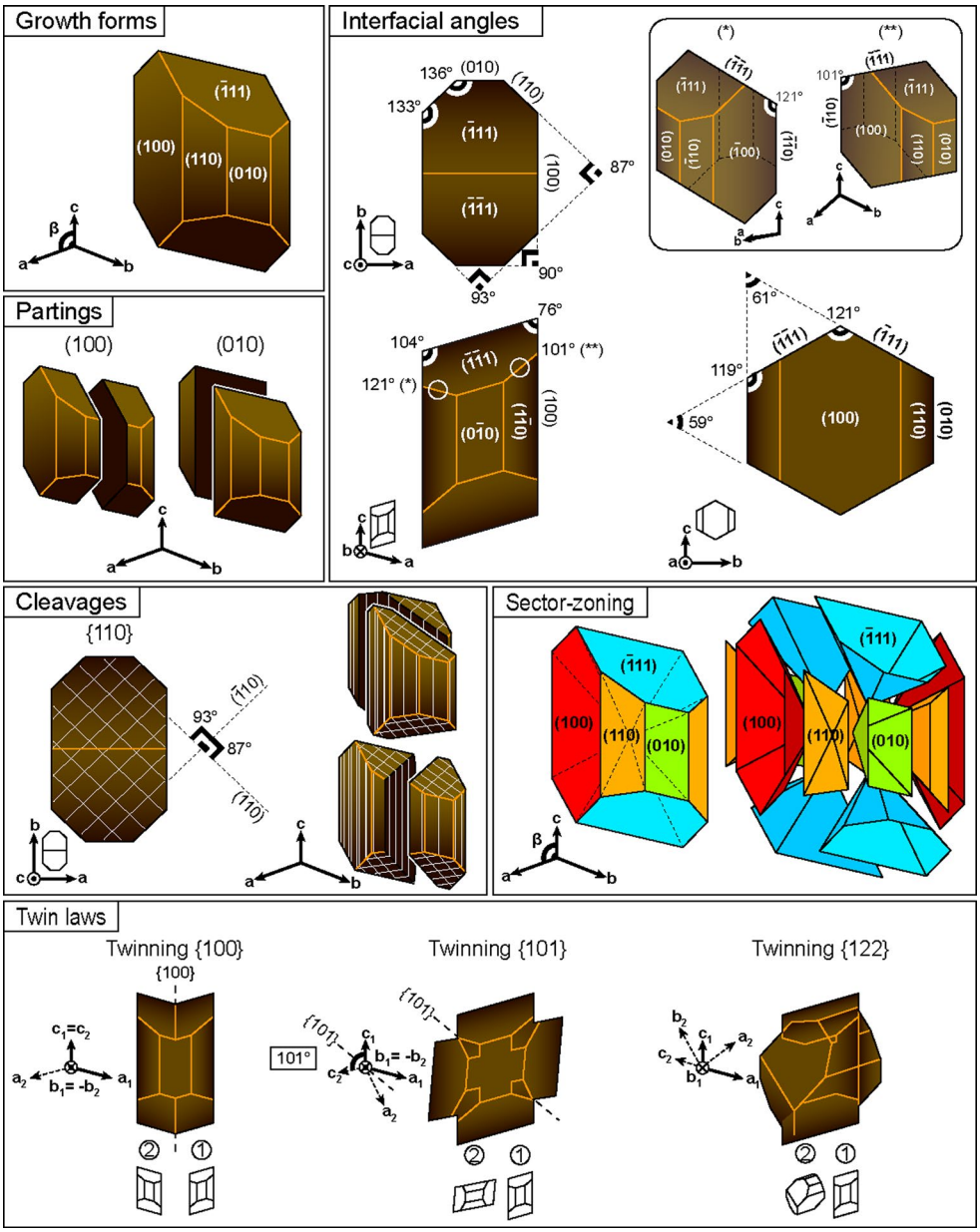

Fig. 2 Mineralogical data for diopsidic clinopyroxene. Crystal model and interfacial angles were calculated using the software SHAPE 7.2 (Dowty 1980, 1987) for pure diopside in the 2/m–C2/c space group with cell parameters $a = 9.746$, $b = 8.899$, $c = 5.251$ Å and $\beta = 105.63°$ (Clark et al. 1969). For an euhedral crystal with an aspect ratio of a:b:c = 1:1.6:1.6 (e.g., webmineral.com), the prominence of the different forms was controlled using reference central distances at {−111} 0.89, {110} 0.90, {100} 0.62 and {010} 1.00. The interfacial angles are invariant whatever the shape ratio (law of constant angles, (Romé de l'Isle 1783; Steno 1669). Computations indicate that clinopyroxene end members (such as hedenbergite and wollastonite) have similar mineralogical data with variations <0.1 Å for the cell parameters a, b and c, <1° for β (Cameron and Papike 1981; Deer 1997) and <0.5° for the interfacial angles. The insert box marked with a (*asterisk*) show the true interfacial angles between the forms {−111} and {010}, which cannot be observed in any other orientation. Good cleavages occur in the plane (110) at ~87/93°. Partings occur in the planes (100) and (010) (Deer 1997). The twinning laws type reflection {100}, {101} and {122} of augite were reported after Rosenbusch (1888). Twins {100} have mutual c-axes but opposite b-axes, yielding an arrow-shaped crystal elongated along the c-axis. Twins {101} form a cross-shaped crystal built on a ~101° rotation around opposite b-axes. Twins {122} form a more complex, cross-shaped crystal. Sector zoning refers to intracrystalline growth domains of pyramidal shape and variable composition (Strong 1969) and references therein). Sectors are pyramidal in shape, having bases that manifest the crystal's external faces and apices that converge toward the crystal's center. A typical augite crystal is made of twelve growth sectors: four {−111}, four {110}, two {100} and two {010}. Their compositional variations result from crystal growth upon structural differences arising at the surface of pyroxene's faces, involving coupled substitutions of the type $(Al + Ti + cations)_{\{hkl\}} = (Si + Mg + cations)_{\{hkl\}}$ (Dowty 1976, 1977; Duncan and Preston 1980; Hollister and Hargraves 1970; Larsen 1981; Nakamura 1973; Shearer and Larsen 1994; Shimizu 1981; Skulski et al. 1994; Watson 1996; Watson and Liang 1995)

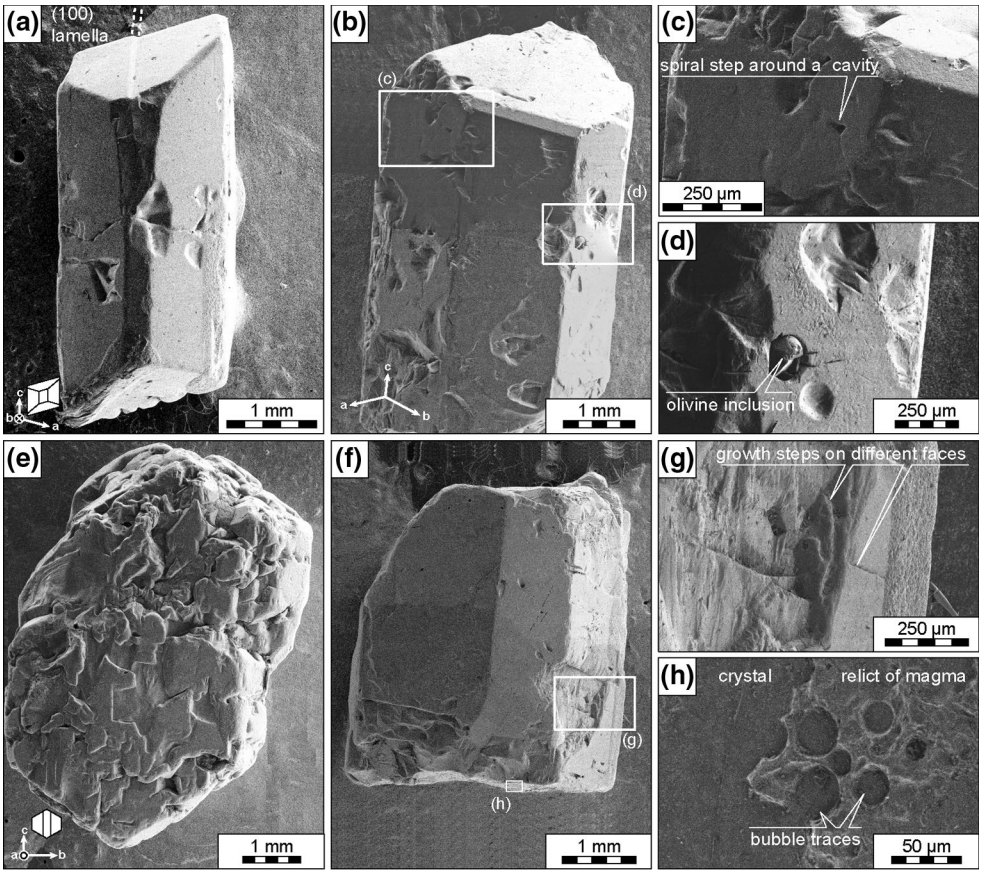

Fig. 3 SEM images of mesostasis-free clinopyroxene phenocrysts: **a** polyhedral phenocryst showing a (100) twin lamella; **b** polyhedral phenocryst showing porous surfaces; **c** phenocryst with a spiral step turning around a cavity, possibly a hollow screw dislocation core; **d** open cavity showing olivine inclusions in clinopyroxene; **e** phenocryst with a markedly uneven surface, made of smaller faceted crystal units, slightly misoriented; **f** broken polyhedral phenocryst; **g** growth steps at the surface of the crystal shown in **f**; and **h** relict of magma at the surface of crystal **f** showing that vesiculation occurred in the melt after clinopyroxene crystallization

misaligned by up to 7°, producing faint extinction discontinuities and variations in interference color within the group as viewed in thin section (Fig. 5f). In some cases, the crystals show undulose extinction.

Mosaicked groups (Fig. 4c) resembling the olivine clusters described by Welsch et al. (2013) are rare, but notably self-similar in terms of surface texture, i.e., there is no group made of both euhedral and spongy units, suggesting that the crystal units of a given group formed in a similar range of magmatic conditions. These crystals are similar to the mosaic block and lineage structure of dendrites described in metallic alloys (Buerger 1932, 1934; Chalmers 1964).

Groups of nonparallel crystal units are commonly related by a twinning law (Fig. 2). Reflection twins on (100) are most frequent (Figs. 1, 4b, c), as previously observed (Washington and Mervin 1922). Twin individuals of this law are typically the same size and comprise a crystal intergrowth slightly elongated along the *c*-axis relative to untwined crystals (for example *a*:*b*:*c*–1:1:1.6 in Fig. 4b). Crystals related by {122} are rarer, and no twin {101} was observed in the samples. Parting is uncommon among the crystals observed in thin section, but parting on (010) is common in the loose samples. The parting plane on loose crystals is fresh and devoid of matrix material, in contrast to crystal growth faces.

The interiors of clinopyroxene crystals are characterized by two textural domains as revealed in thin section crossed-polars photomicrographs (Fig. 5), X-ray element intensity maps (Figs. 6, 7a, b), BSE imagery (Fig. 7c, d) and reflected light (Fig. 7e, f): irregularly porous "spongy" domains and laterally continuous "nonspongy" domains. The clinopyroxene in the spongy domains has slightly lower optical retardation (Fig. 5) and lower Z-contrast values than in the solid zones (Fig. 7c, d). The pores are variably occupied by matrix material, similar to features described in clinopyroxene of arc volcanics (Streck 2008; Streck et al. 2002, 2005). This porosity occurs at the cores of crystals (Fig. 5c), at their margins (Fig. 5a), and sometimes throughout entire crystal sections (Figs. 5e, 7e). In contrast to the correlations

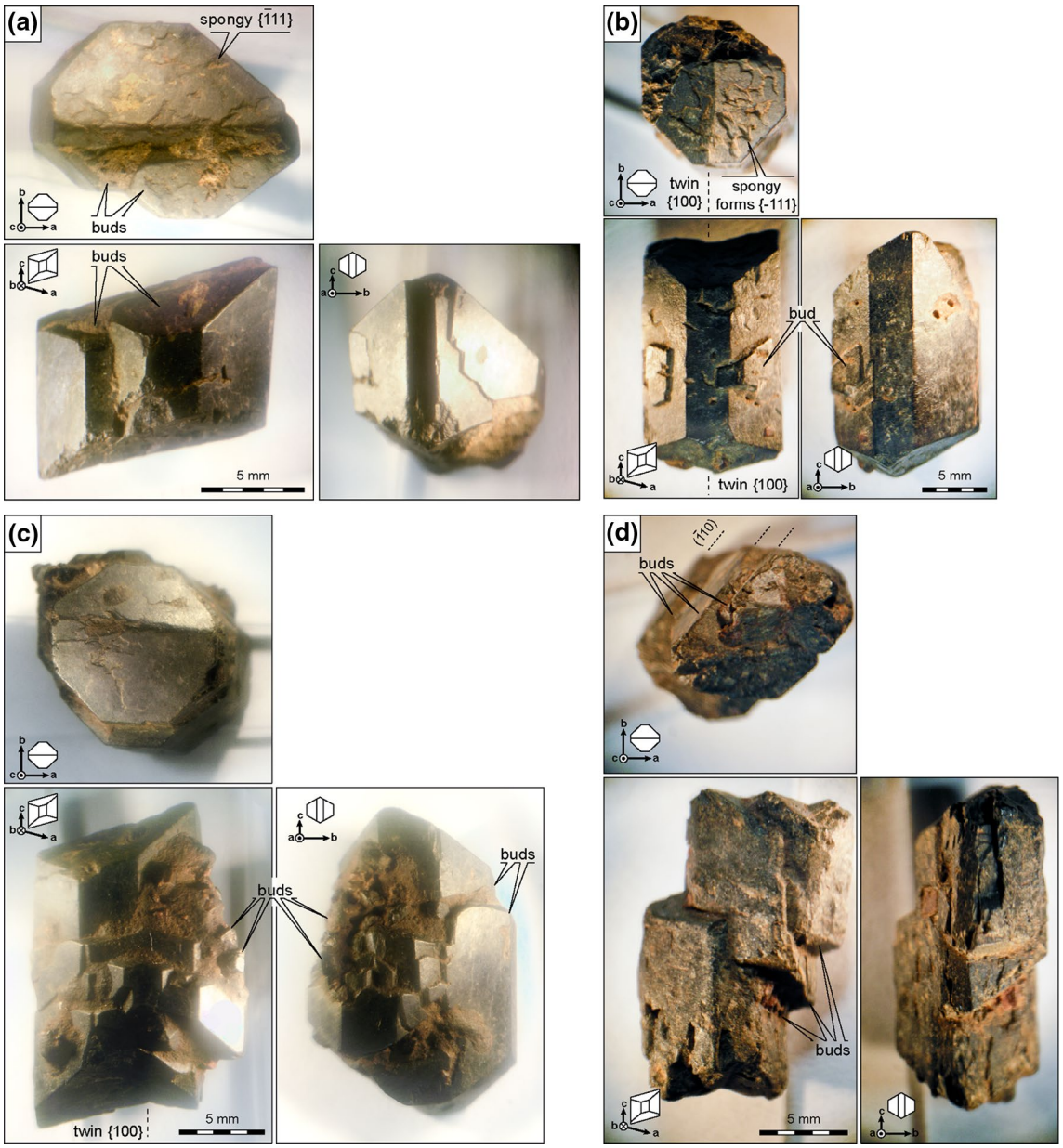

Fig. 4 Textures of mesostasis-free clinopyroxene phenocrysts (each phenocryst was photographed with a stereomicroscope in the three primary directions [100], [010] and [001]): **a** phenocryst made of two parallel crystal units or "buds"; **b** twins {100} showing two buds at their surface, yielding a blocky and mosaic texture; **c** phenocryst made of many buds and one twin {100}, resulting into a mosaicked texture; **d** phenocryst composed of three buds slightly misoriented. Note that all the faces have an irregular, porous surface in this specific crystal. In contrast, all forms {hk0} are well faceted and have a smooth surface in the crystal units of **a**, **b** and **c** phenocrysts; and only their forms {−111} show vermicular "spongy" macrosteps at their surface

described above for the loose 3D crystals, the spongy zones generally occur beneath the {hk0} external growth forms, and the nonspongy zones tend to be situated beneath the faces of form {−111} (Figs. 5, 6). Lack of downstream scratches, surface topography or other imperfections indicate that the porosity itself does not result from thin section preparation and is a primary feature of the clinopyroxene phenocrysts. However, breakage features within the porous areas suggest that much of the space now occupied by epoxy was formerly occupied by matrix material, i.e., it is likely that only a small proportion of the pore space within the spongy domains represents magmatic vapor bubbles. Cavities produced by sample preparation are typically irregular in shape, presumably outlining mechanical weaknesses at the boundaries of phases. In contrast, vesicles are rounded due to surface tensions at the melt–vapor interface

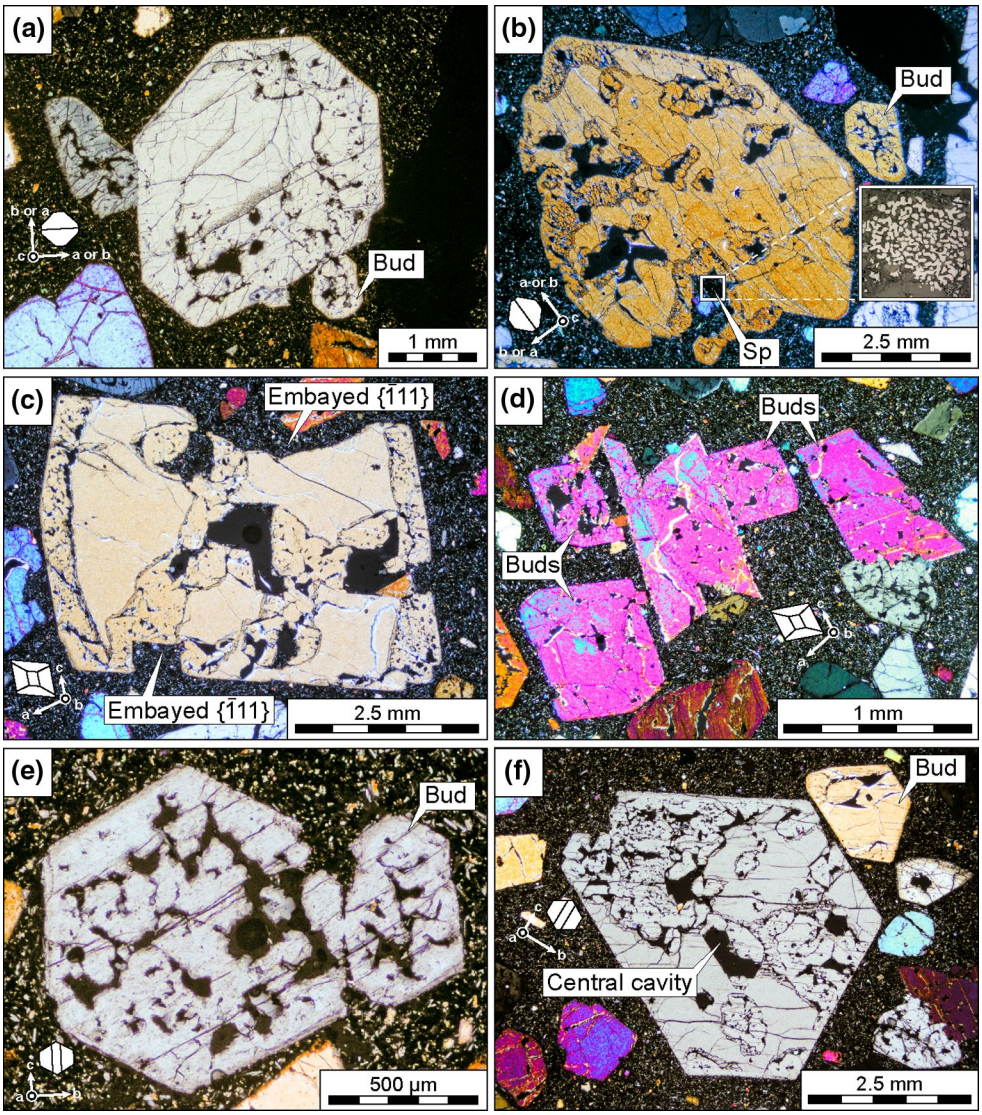

Fig. 5 Textures of clinopyroxene phenocrysts in thin sections (transmitted light photomicrographs with crossed polars): **a** parallel group of three crystal units; **b** large crystal showing several spongy domains. Spinel shown in reflected light; **c** crystal showing irregular contact between spongy and nonspongy domains. The spongy domains near the outermost rims are remarkably parallel to the forms {hk0}. Note also the faceted embayment at the *bottom* and the curved embayment at the *top*; **d** crystal made of at least three parallel subcrystals; **e** crystal made of two parallel subcrystals with large spongy domains; **f** crystal made of two subcrystals. The variation in the optical retardation of the bud (in *yellow*, *top right corner*) indicates slight deviation from perfect alignment with the larger unit. Note that all the crystals in **a**–**f** show examples where both nonspongy and spongy domains are in contact with the mesostasis. Mineral abbreviations are given after Kretz (1983)

during exsolution of volatiles. Both damaged surfaces and vesicles can be either empty or filled with epoxy, depending on the success of the epoxy impregnation.

Pockets within clinopyroxene that contain matrix material range in size from 10 to 200 µm and enclose glass, plagioclase, olivine, spinel and ilmenite crystals (Figs. 5, 6, 7). The olivine crystals have a macro- to mesocryst size with an anhedral shape when in contact with clinopyroxene, and a polyhedral, faceted shape when in contact with the mesostasis (Figs. 7d, 8c, d). The compositions of olivine inclusions are similar to those of olivine phenocrysts located in the mesostasis. Spinel is absent in the mesostasis surrounding clinopyroxene phenocrysts. The spinel microcrysts in the clinopyroxene phenocrysts have a cubic, octahedral or spongy morphology (Figs. 5b, 11).

Hammer et al. (this issue) demonstrated that quantitative EPMA spot analyses, despite numbering several dozen per crystal, alone are insufficient to demonstrate a statistically significant correlation between composition and texture domain type. Evidently, the variance within domains

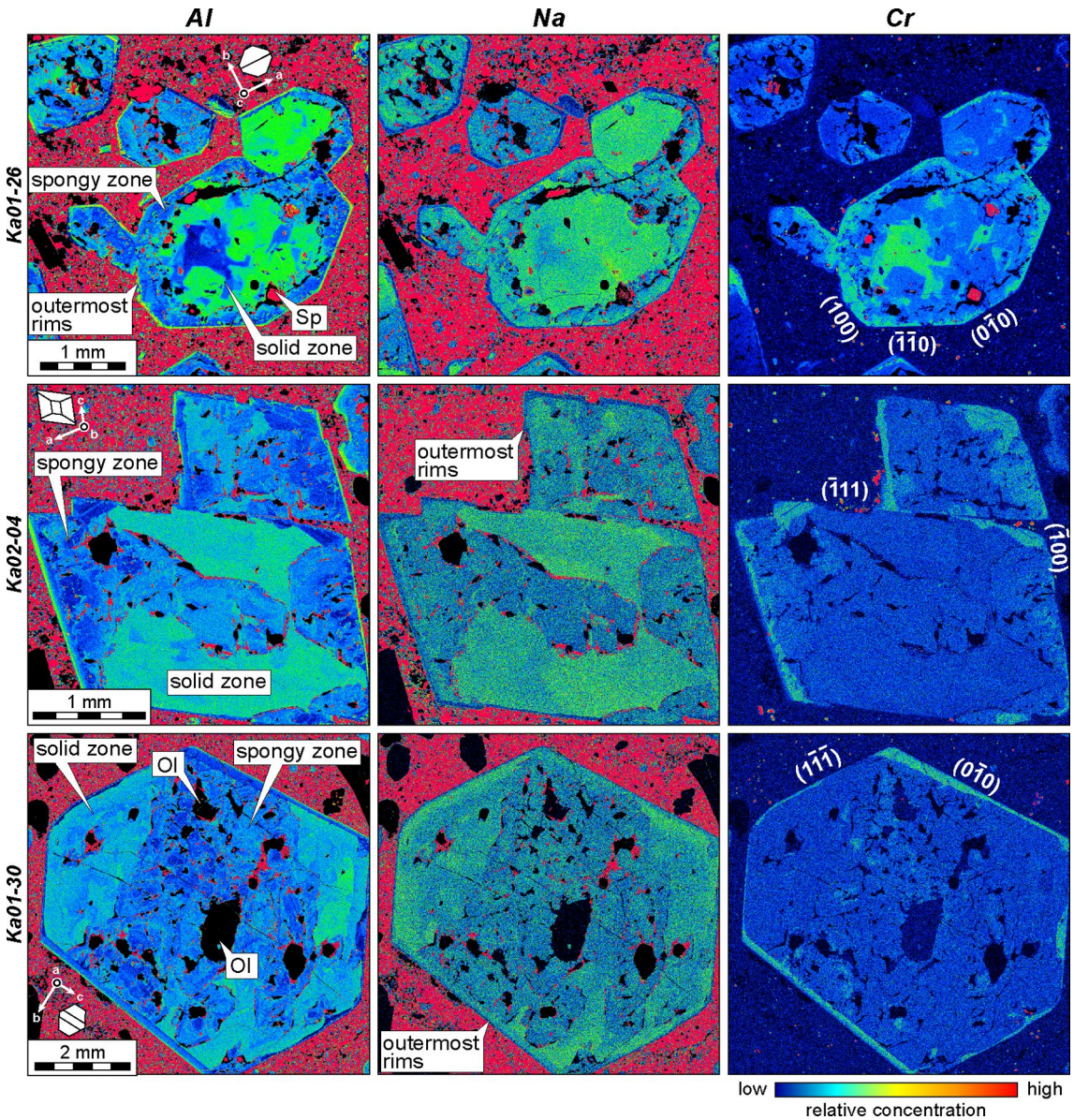

Fig. 6 X-ray distribution maps of three clinopyroxene phenocrysts (Ka01-26MCK, Ka02-PNK and Ka01-30). All three crystals show domains enriched in Al and Na anti-correlated with domains enriched in Cr. Note the occurrence of crystallographically aligned subcrystals ("buds") in crystals Ka01-26MCK and Ka02-PNK. The crossed polarized pictures of these three crystals are given in Fig. 11. See also the Supplementary Materials for additional maps in Haleakala clinopyroxene

is so large as to obscure a small but consistent difference between the mean compositions. However, the high spatial sampling frequency afforded by X-ray intensity mapping in this study (Figs. 6, SM1 and 2) clearly reveals intracrystalline variations in Si, Al, Mg, Ca, Na, Ti and Cr that are linked to texture type. The chemical variations correlate precisely with the solid and spongy domain types: nonspongy zones associated with the external {−111} faces are enriched in Al, Ti and Na, and the spongy domains capped by {100}, {010} and {110} faces are enriched in Si, Mg, Cr and Ca. The element maps further indicate that the spongy domains are compositionally heterogeneous at a finer scale with different spatial distributions than in the nonspongy domains. Within nonspongy areas, the variations are blocky rectangular (e.g., center part of crystal Ka01-26 and majority of Ka02-22) with clear anti-correlation of Al and Cr (Figs. 6, SM1 and 2). Within intraspongy domain, variations appear more chaotic and even fluidal in character (Fig. 7). A second-order observation is that within the spongy domains, the concentrations of Si, Mg, Ca and Cr domains gradually increase toward the outside of crystals, stopping short of the outermost 30 μm (Table 1;

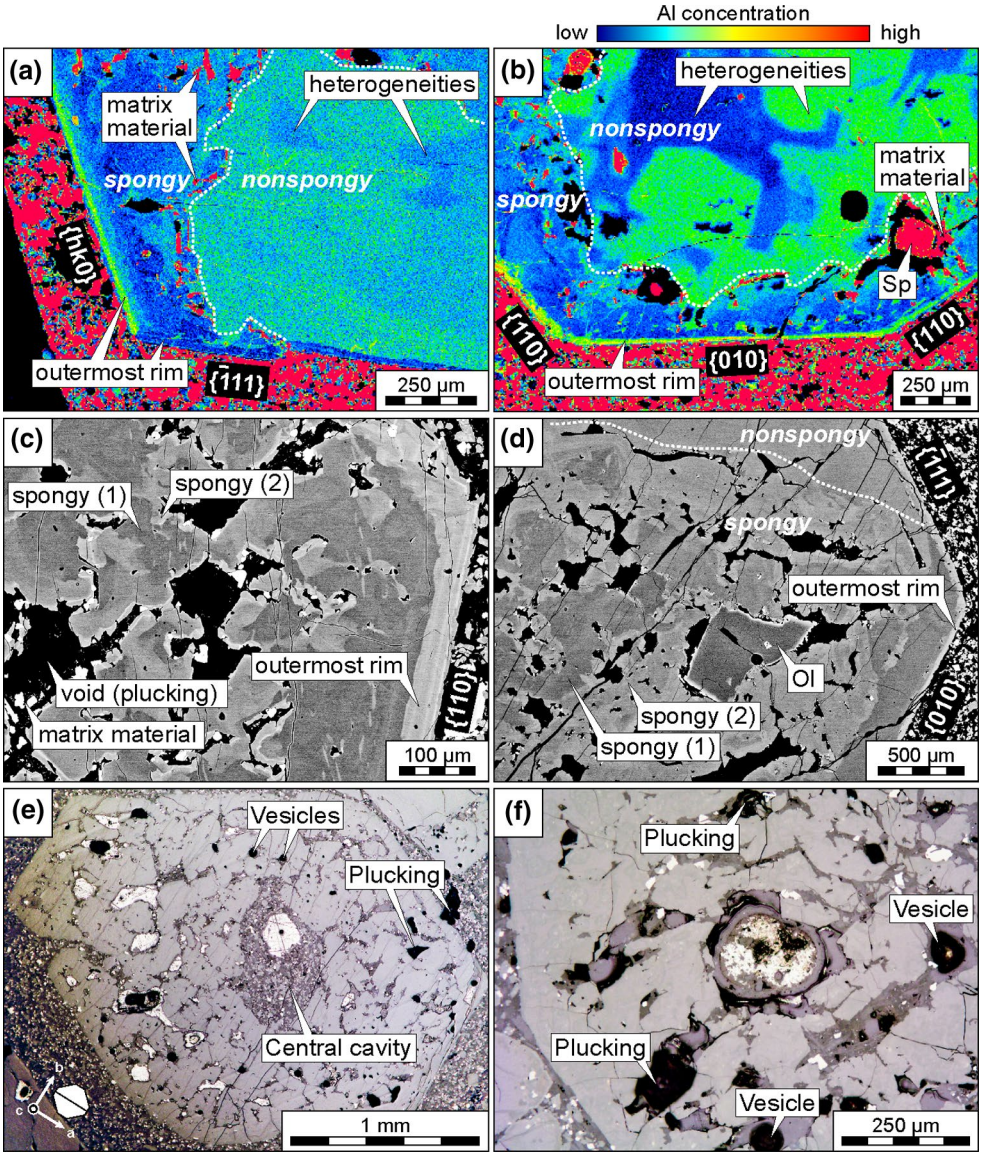

Fig. 7 Al-kα distribution maps (**a**, **b**) and BSE images (**c**, **d**) of four clinopyroxene phenocrysts showing chemical heterogeneities within nonspongy sectors {−111} and spongy sectors {100}, {010} and {110}. The *bright zones* labeled "spongy (2)" are in contact with the matrix material, which suggest that they grew last as overgrowths on the *darker areas* labeled "spongy zones (1)". The *dark areas* within the spongy sectors {100}, {010} and {110} initially contained matrix material that was plucked during thin section preparation (pits observed in reflected light). Remnants of the matrix material can be observed at the contact with the *bright zones* labeled "spongy (2)." **a** crystal Ka02-04; **b** crystal Ka01-26; **c** crystal Ka02-17; and **d** crystal Ka01-30. **e** and **f** are two reflected light microphotographs showing the position of vesicles and plucked surfaces within the clinopyroxene phenocrysts

Figs. 6, 7). For example, the Cr increases toward the margins of Ka01-26 (Fig. 6) and then decreases abruptly within the outermost rims. The Mg concentrations in crystal Ka02-04 increase from the center to the rim within the spongy domain associated with the form {100} and then drop in the outermost rim (Fig. SM1). Slight enrichment in V is evident at the outermost rims of clinopyroxene macrocrysts (Fig. SM1).

The element concentration maps also reveal abrupt compositional shifts near the crystal–mesostasis boundaries, but with orientation effects present for some elements and not others. Whereas the outer ~30 µm, here termed "outermost rims," is depleted in Na and Cr regardless of face form, the concentrations of Al and Ti are enriched on the {100}, {010} and {110} faces, while Si, Mg and Ca are enriched on the {−111} faces (Fig. 6). This element correlation pattern represents a direct reversal with respect to the immediately underlying crystalline material described above. The reversal in element partitioning on form types is in fact consistent with the reversal in textures of various faces revealed by the 3D (surface) and 2D (interior) observations. That is, the spongy texture is consistently associated with elevated Si, Mg and Ca, whereas the nonspongy is consistently higher in Al and Ti. The correlation between composition and texture persists, whether a given texture occurs on the {hk1} form or on the {hk0} forms.

Olivine phenocrysts

The olivine phenocrysts have a texture similar to those described in ocean island basalts, picrites and oceanites (Helz 1987; Welsch et al. 2013). They occur as isolated crystals or

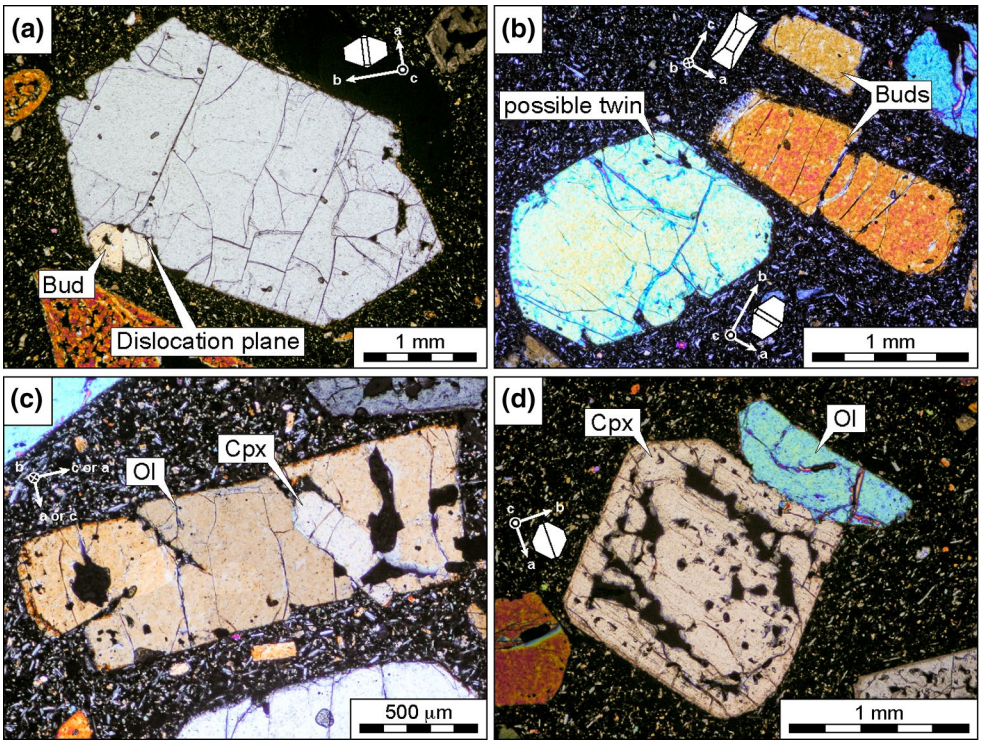

Fig. 8 Textures of olivine phenocrysts in thin section (photomicrographs with crossed polars): **a** euhedral crystal showing a subgrain with slight optical retardation due to a small deviation from perfect crystallographic alignment; **b** crystal made of two parallel subcrystals and one suspected twin (all three units have a simultaneous extinction); **c** intergrowth of clinopyroxene in an olivine crystal (n.b. the faces cannot be distinguished through the method of interfacial angles in this type of section); and **d** intergrowth of olivine and clinopyroxene

Table 1 Principal characteristic of Haleakala clinopyroxene

Crystal	Forms {−111}	Forms {100}, {010} and {110}	Interpretations	Implications
Interiors	Solid texture Al, Ti, Na rich Si, Mg, Ca, Cr poor	Spongy texture Si, Mg, Ca, Cr rich Al, Ti, Na poor	Rapid growth at depth	High supersaturation in the reservoir
Outermost rims (<50 µm)	Plateaued surface Mg, Ca, (Si) rich Al, Ti, Na, Cr poor[a]	Smooth surface Al, Ti rich Na, Si, Mg, Ca, Cr poor[a]	Slow growth at the surface	Lower supersaturation in the lava flow

[a] The outermost rims are uniformly depleted in Na and Cr

as groups in which individuals are related by a special crystallographic orientation. The subcrystals are variously euhedral, rounded, twinned and/or embayed with local lattice misorientations at their junctions (Figs. 8, 9). Edges in contact with the mesostasis are slightly iddingsitized. Some crystals contain crystalline inclusions and spinel microcrysts. Olivine can enclose clinopyroxene (Fig. 8c) or be enclosed by clinopyroxene (Figs. 6, 7d, SM1). X-ray element maps of P, Cr, Al and Ti reveal flat concentrations throughout, with the exception of weak lamellar P enrichments (Fig. 9).

Discussion

Key observations from the 3D morphological and 2D morpho-compositional study of Haleakala clinopyroxene are summarized in Table 1, along with preferred interpretations. Each piece of evidence is considered separately and then combined as it pertains to clinopyroxene supersaturation to develop a conceptual model for the growth history of crystals in the Haleakala magma reservoir.

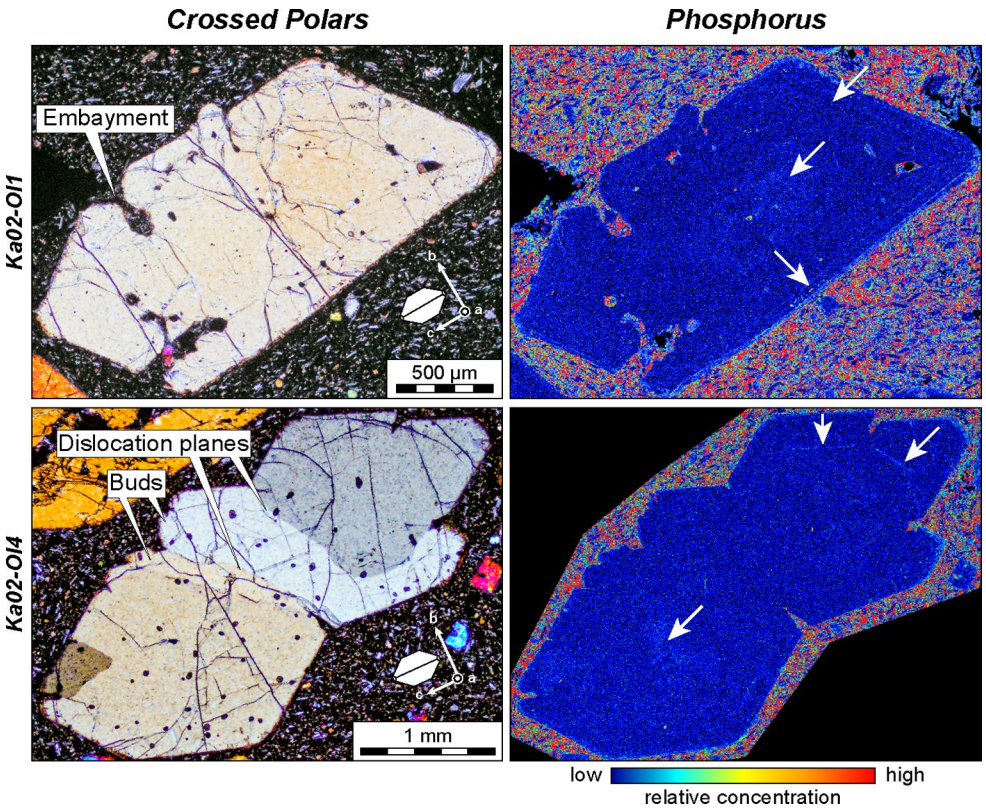

Fig. 9 Transmitted light microphotographs with crossed polars and corresponding phosphorus distribution maps of two olivine phenocrysts showing spatially sharp, small amplitude P enrichments near their outermost rims and at their centers

Parallel groupings

The occurrence of groups of crystals is a first-order feature of the Haleakala ankaramite that can be interpreted in several ways. One interpretation is that each subcrystal had a different origin in the magma before coalescence into a polycrystal, as has been suggested to occur for olivine (Schwindinger 1999; Schwindinger and Anderson 1989) and plagioclase (Kuo and Kirkpatrick 1982; Stull 1979). However, this idea is inconsistent with the observation that crystal units of a given group have a similar habit (Fig. 5), which suggests a common history in the magma. More importantly, the crystallographic alignment of subunits is unlikely to occur by impingement in viscous silicate melt. Heterogeneous nucleation, crystal aggregation and synneusis are also unlikely to produce cascades of self-similar crystals (Fig. 4d) or mosaicked textures (Fig. 4c).

Because the characteristics of the Haleakala clinopyroxene are similar to ordered textures reported in olivine from Piton de la Fournaise, which were interpreted to result from initially dendritic crystallization at high supersaturation (Welsch et al. 2013), we consider whether the interpretation developed for olivine is applicable to Haleakala clinopyroxene. The observation that the subcrystals of clinopyroxene phenocrysts have parallel faces and continuous optical orientation, even when separated by mesostasis (Fig. 5b, d, f), is consistent with the possibility that they represent branched protrusions from a single crystal during early dendritic growth (Sunagawa 2005; Wadsworth 1961). We interpret each polycrystal as having formed by a single nucleation event. The subordinate units are buds, which in some cases coarsened apart from the parent crystal, but also frequently became intimately intergrown with the parent.

Twins

It is important to note that the polycrystals are distinct from twins, which manifest nonparallel alignments such as mirrored orientations for twins on (100) and tilted orientations for twins on (122); Figs. 1 and 4. According to Buerger (1945) and shown experimentally for plagioclase in rhyodacite magma (Brugger and Hammer 2015), twins tend to form as growth defects when crystals are still small (<10 µm) and that this tendency to form twins increases with supersaturation. The prevalence of equal-sized twin intergrowths among Haleakala clinopyroxene crystals is consistent with initially high supersaturation and rapid growth.

Spongy texture

The presence of internal cavities filled with matrix material (Figs. 5, 6, 7) is a striking feature of the clinopyroxene phenocrysts that distinguishes them from the olivine crystals in the host ankaramite. The occurrence of discrete spongy domains that are sharply defined with respect to nonspongy regions also motivates the question of how they formed and in what environmental conditions.

The spongy domain is unlikely to be the result of partial dissolution (e.g., caused by magma mixing or re-heating) because dissolution involves detachment processes at the crystal–melt interface and alone cannot lead to a preferential destabilization of the crystal's interior. For instance, the dissolving crystals in the experiments of Kuo and Kirkpatrick (1985) are externally rounded but internally nonspongy, which contrast with the planar faces and the spongy interior of the Haleakala clinopyroxene (Figs. 1, 3, 4, 5, 6, 7). A scenario of partial dissolution followed by the development of polyhedral overgrowths is also unlikely since both spongy and nonspongy domains of crystals are in contact with the matrix (Figs. 5, 6, 7a, d). Importantly, the nature and significance of spongy domains is intimately associated with intracrystalline compositional heterogeneity, as explored below. One thing is certain—the spongy domains represent areas of particularly high crystal–matrix interfacial area, and thus relatively high energy compared with the compact euhedral crystals expected to form near equilibrium. The occurrence of a central, faceted cavity in several phenocrysts (Figs. 5f, 7e) is especially consistent with rapid growth. Skeletal and dendritic crystals show similar cavities in sections parallel to their faces, and these are described as reentrant faces (Faure et al. 2003a; Sunagawa 2005; Ni et al. 2014). Such features represent a transition between growth regimes: one in which apices propagate forward to pierce compositional boundary layers, and another in which growth propagates backward to fill cavities that are no longer energetically sustainable because thermodynamic supersaturation has decreased. For instance, internal sponginess can be observed in skeletal and dendritic crystals grown at high cooling rates (Fig. 3b, c in Lofgren et al. 2006).

Vesicles trapped in the spongy domains indicate volatile saturation in the magma during or after growth of the crystal interiors (Fig. 7e, f). A first possibility is that the bubbles formed on the crystal surface by heterogeneous nucleation, upon decompression during the eruption. A second possibility is that the entire reservoir was saturated, but perhaps more likely is that volatile saturation was achieved in crystal mushes or within the boundary layers of rapidly growing clinopyroxene.

Spatial correlation of texture and composition

Without knowledge of crystallographic orientation, the observed textural domains and correlative compositional domains appear not only highly variable between crystals but also randomly distributed within crystals (Figs. 5, 6, SM1 and 2). However, a pattern emerges when the domains are viewed as groupings of sectors within clinopyroxene. Figure 10 presents a model of a hypothetical Haleakala clinopyroxene, in which {−111} sectors are distinguished from the {100}, {010} and {110} sectors. The 2D sketches of the domain distributions that result from slicing the crystal along principal planes at different distances from its core are presented as predictions against which natural crystals may be compared. In some slices, including both near-center cuts (e.g., perpendicular to *c*-axis, at C1) and near-edge cuts (e.g., perpendicular to the *a*-axis, at A3), the crystal sections are dominated by the {−111} sector. In other slices, the {hk0} sectors rim the {−111} sectors, appearing to concentrically mantle a core of the opposing domain (C2). In the majority of slices, both domain types appear at the interiors as well as edges of the crystal (A1–A3, B1–B3 and C3), illustrating the existence of disparate domains simultaneously in contact with surrounding melt. Naturally, nonprincipal sections would produce an even more diverse set of relationships (e.g., Figure 5a, b).

These zoning patterns are compared in Fig. 11 to the zoning patterns of the observed clinopyroxene crystals, utilizing the independently determined crystallographic orientations. The boundaries between domains are neither linear nor highly symmetric, as in the idealized drawings. However, the similarities between the zoning patterns of the models and those of the natural crystals exceed the differences and, moreover, are remarkably consistent among all crystals exhibiting indexed faces. These similarities strongly suggest that the nonspongy and spongy domains of the natural clinopyroxene (Figs. 5, 6, SM1 and 2) correspond to the sector groupings, as follows: (a) nonspongy sectors {−111}, enriched in Al, Ti and Na, and (b) spongy sectors in the {hk0} family, {110}, {100} and {010}, enriched in Si, Mg, Cr and Ca (Figs. 10, 11).

Observations in synthetic (Kouchi et al. 1983; Lofgren et al. 2006) and natural sector-zoned crystals (Downes 1974; Duncan and Preston 1980; Hollister and Gancarz 1971; Hollister and Hargraves 1970; Leung 1974; Strong 1969; Wass 1973) suggest that the compositional variations of clinopyroxene sectors are fairly consistent across magmatic affinities and clinopyroxene major element composition, with Al and Ti concentrated in one set of sectors, and Si and Mg concentrated in a different set of sectors. The other cations (including Fe, Ca and Na) exhibit a more complex behavior and variably appear in the Al–Ti-rich sectors and the Si–Mg-enriched sectors, possibly reflecting

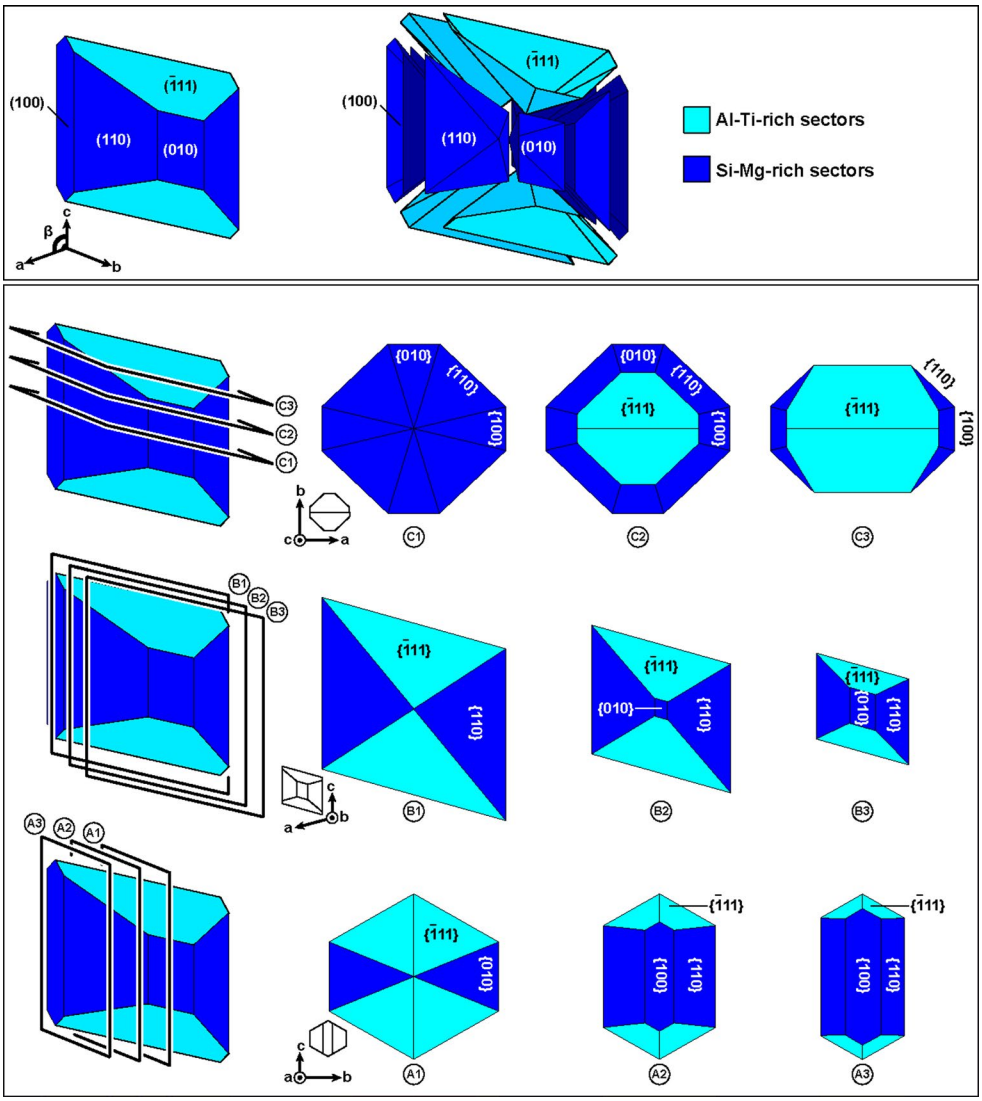

Fig. 10 Sketch of zoning patterns obtained as a function of the cut orientation and depth in a sector-zoned crystal of clinopyroxene, using the same color code as in the chemical maps (see also Downes 1974; Ferguson 1973; Leung 1974; Wass 1973 for other examples of cut effect). The morphology of the crystal model is based on the crystal units of Fig. 4a with a shape ratio *a*:*b*:*c*–1.08:1:1, using central distances at {−111} 0.78, {110} 0.86, {100} 1.00 and {010} 0.92. *Light blue tones*: solid sectors {−111} enriched in Al, Ti and Na. *Dark blue tones*: spongy sectors {100}, {010} and {110} enriched in Mg, Si, Cr and Ca. All the subdivisions between the sectors are outlined here, although they cannot be observed in natural crystals when the sectors have similar composition and texture (e.g., {100}, {010} and {110}, or two sectors {−111} in Haleakala crystals). The zoning patterns are shown following serial cuts in a perfect crystal model, progressing from the center of the crystal (A1, B1 and C1) toward its peripheries (A2, B2, C2, then to A3, B3 and C3, respectively). It is important to note that sections type C2 [i.e., near the plane (001)] produce apparent concentric zoning

incorporation by coupled substitution and/or charge compensation. The experiments of Kouchi et al. (1983) show that the composition of clinopyroxene is not only sensitive to the cooling and supersaturation conditions, but also that there is not only one, but *several* types of sector zoning. In their experiments, Al and Ti are concentrated in the sectors {100} at $-\Delta T = 13$–18 °C, in the sectors {110} at $-\Delta T = 25$ °C and in the sectors {−111} at $-\Delta T = 45$ °C (Fig. 12). In the volumetrically dominant interiors of the Haleakala clinopyroxene crystals, the type of sector zoning is $(\mathrm{Al} + \mathrm{Ti} + \mathrm{Na})_{\{-111\}} = (\mathrm{Si} + \mathrm{Mg} + \mathrm{Cr} + \mathrm{Ca})_{\{110\},\{100\},\{010\}}$, which is similar to that observed in the synthetic crystals grown at high degrees of supersaturation ($-\Delta T = 45$ °C, Fig. 12), and also to that observed in the crystals of the 1669 eruption at Mount Etna (Downes 1974). The identification of this type of sector zoning in the interiors of Haleakala clinopyroxene is therefore another piece of evidence in support of early rapid growth at high supersaturation.

The petrographic characteristics of olivine phenocrysts in the ankaramite also are consistent with rapid crystallization. Their subdivided structure into subparallel units (Figs. 8a–c, 9) and their P-rich zoning (Fig. 9) are both evidence of dendritic growth at high degree of supersaturation ($-\Delta T > 60$ °C), provided that diffusion-limited growth promotes the formation of protrusions and the incorporation of slow-diffusing impurities such as P, Al and Cr (Faure et al. 2003a, b; Milman-Barris et al. 2008; Welsch et al. 2013, 2014). The fact that both rapid-grown olivine and clinopyroxene have intergrowth relationships (Fig. 8c, d) indicates that the whole parental magma of the ankaramite began to crystallize in conditions far from equilibrium prior to eruption.

Finally, we consider the reversal in both the distribution of spongy and nonspongy domains and compositional element covariation with respect to sector grouping in the outermost ~30 μm rims of the clinopyroxene crystals. Here

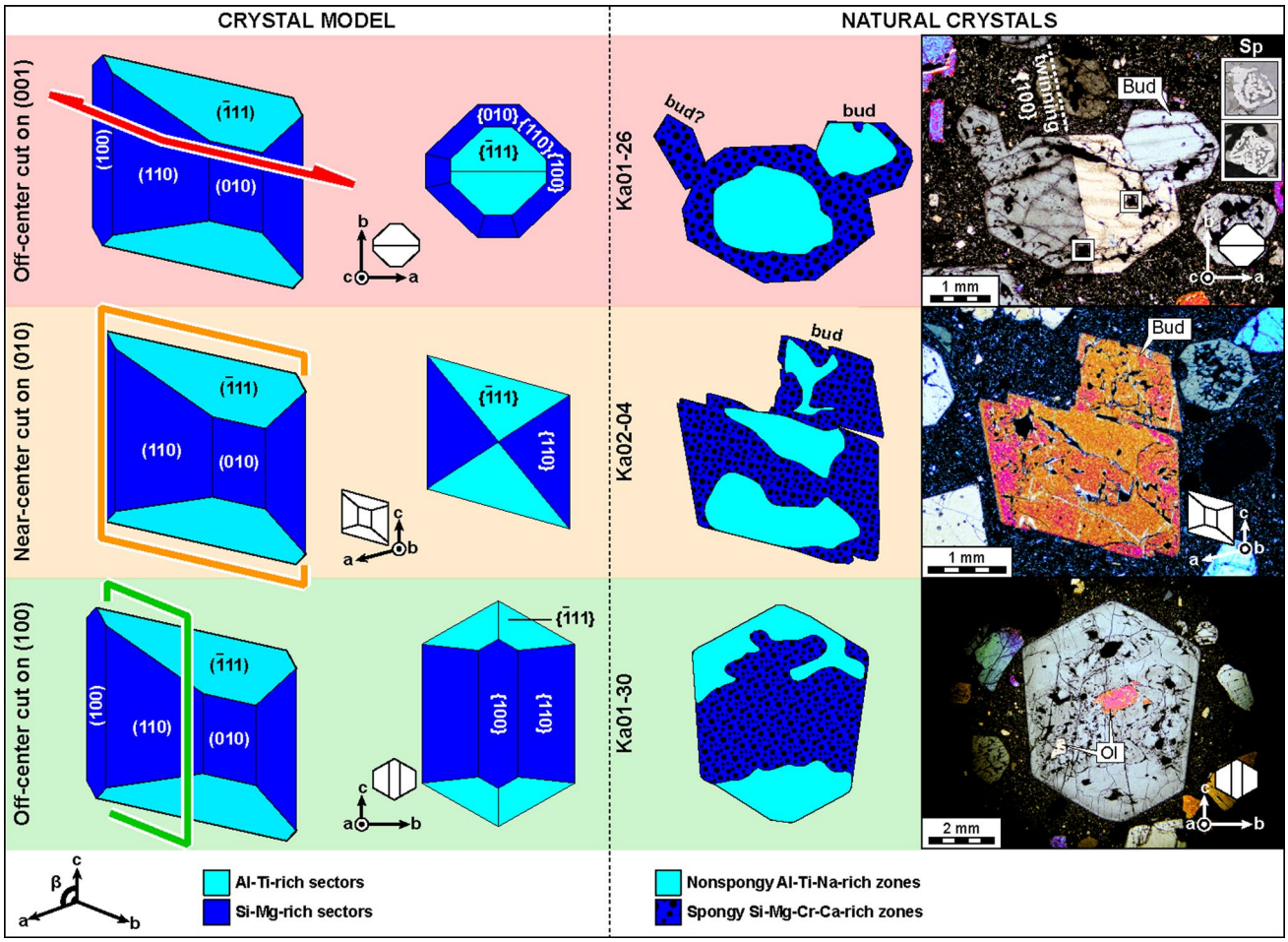

Fig. 11 Comparative sections of a modeled sector-zoned crystal and phenocrysts from Qkuls ankaramite, taking into account their crystallographic orientations. Except for the presence of buds, twins and the vermicular texture of sectors {100}, {010} and {110} (outlined in *dark blue areas*), the zoning patterns of natural crystals are similar to those of the crystal model. Chemical maps of the three natural crystals are given in Figs. 6 and SM1

also, the Kouchi et al. (1983) experimental findings provide a means of interpreting this switch. The experimental crystals have Al and Ti concentrated in {100} at $-\Delta T \leq 18$ °C. We infer that the patterns observed in the Haleakala clinopyroxene are consistent with growth of the outermost rims at relatively low supersaturation compared with the interiors.

Evolving conditions of crystal growth

Several lines of evidence support initial growth of Haleakala clinopyroxene at relatively high degrees of supersaturation. However, the external polyhedral forms of isolated single clinopyroxene crystal unit (Figs. 1, 3a, b, f, 4a–c, 6, 7) suggest that crystals approached their present size and shape via growth at low degrees of supersaturation (Kirkpatrick 1975; Sunagawa 1981, 2005). Taken in aggregate, the internal and external textures suggest that the crystals experienced composite growth history, where polyhedral overgrowths developed slowly on rapid-grown skeletal and dendritic frameworks. This later step of slower growth promoted the filling-in of reentrant faces and protrusions.

Fortunately, we can probe further into the development of these crystals thanks to dynamic crystallization experiments indicating relative rates of growth on different sectors. At large degree of supersaturation, the Al- and Ti-rich sectors {−111} grow faster than the other sectors (Kouchi et al. 1983). Because of this difference in the growth rates of faces, it is probable that these sectors {−111} build and begin to backfill a skeletal structure before maturation of the other sectors occurs. The interpretive model in Fig. 13 presents a possibility that is consistent with the experimental data on face growth rates as well as the presence of spongy textured regions in the natural crystals. First, the sectors {−111} develop at the onset of crystallization at growth

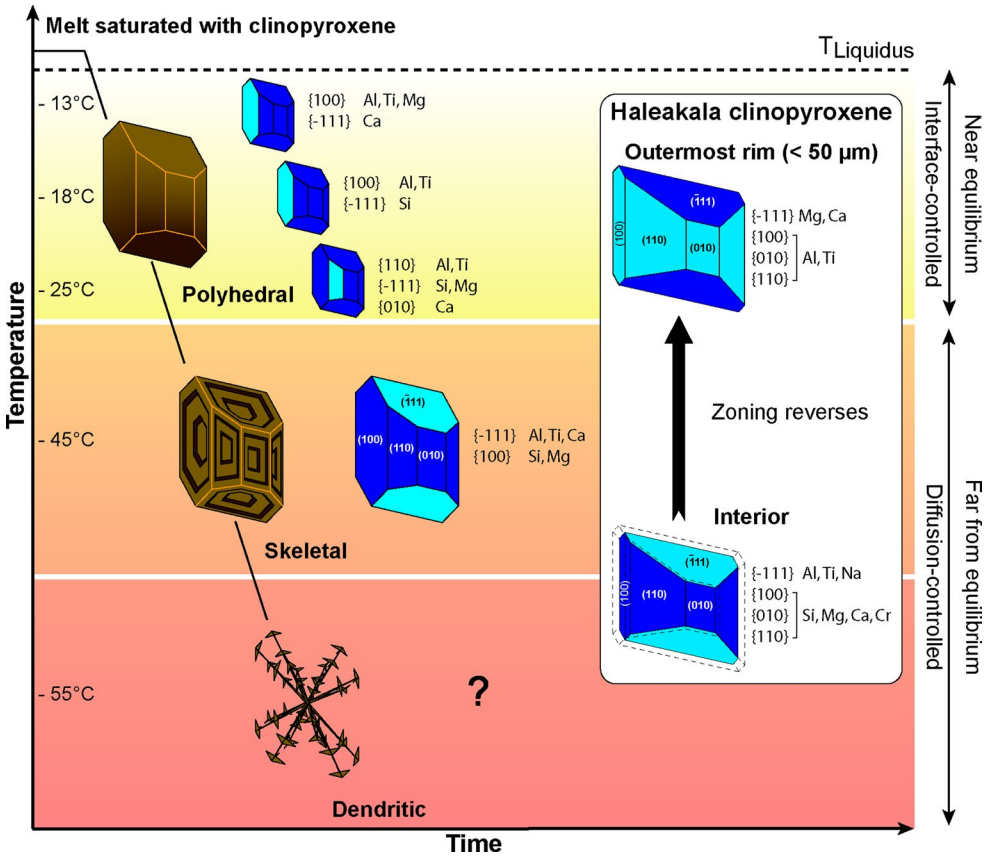

Fig. 12 Crystal morphology and sector zoning in clinopyroxene obtained as a function of the degree of supersaturation ($-\Delta T$) in the system $CaMgSi_2O_6$–$CaTiAl_2O_6$ (modified after Kouchi et al. 1983). The relative chemical enrichment of sectors faces {−111}, {100}, {010} and {110} is displayed to the right of the crystals. The Al-rich and Ti-rich forms are highlighted in *light blue*; the forms enriched with the other elements (Si, Mg and/or Ca) or showing no preferential enrichment are in *dark blue*. Importantly, the type of sector zoning observed in Haleakala clinopyroxene is different from the sector zonings of euhedral crystals formed at low degrees of supersaturation ($-\Delta T$ = 13–25 °C), but similar to sector zoning of skeletal crystals grown at high degrees of supersaturation ($-\Delta T$ = 45 °C). Regarding the discrepancies, the fact that the forms {−111} are enriched in Ca in Haleakala clinopyroxene and not in the experimental crystals may result from the difference in the starting melt composition (complex in natural melts vs. simple in the experimental melt). It is also possible that Haleakala clinopyroxene experienced higher degrees of supersaturation ($-\Delta T \geq 55$ °C; dendritic stage), although Kouchi et al. (1983) were unable to provide the type of sector zoning of dendritic diopside due to the fibrous nature of crystals

rates ~10^{-6} m/s. This is followed by growth on the sectors {110}, {100} and {010} at rates of 10^{-7}–10^{-8} m/s (Kouchi et al. 1983). All the sectors are backfilled as the growth rates decline in response to decreasing supersaturation, with growth rates ~10^{-9} m/s for all sectors. According to the experiments of Kouchi et al. (1983), the type of sector zoning should evolve as the composition of the melt varies and the supersaturation decreases in the magma (Faure and Tissandier 2014), resulting in the formation of compound sectors. We suggest that the chemical heterogeneities observed within the sectors {−111} and {hk0} (Fig. 7a–d) captured such fluctuations as the mineral switched its growth mechanism from diffusion to interface controlled at depth. The vermicular domains labeled "spongy (1)" may correspond to the first dendritic architecture of sectors {hk0} overgrown by the domains labeled "spongy (2)."

The internally spongy texture of sectors {110}, {100} and {010} suggests that backfill on these sectors was interrupted by the eruption and freezing of magma at the surface. However, the faster growth on {−111} allowed these sectors to completely backfill, producing nonspongy texture on these faces. The external spongy textures on other sectors of some crystals (Figs. 3e, 4d) likely correspond to juvenile growth morphologies arrested at the transition between rapid and slow growth, as has been suggested for the existence of curved surfaces on growing olivine (Welsch et al. 2014).

Anisotropy of growth rates on different faces, as we invoke to explain why some sectors are spongy and others not, is similar to a previous hypothesis for the origin of "hourglass" clinopyroxene (Faquhar 1960; Gray 1971; Leung 1974; Rosenbusch 1888; Skulski et al. 1994; Strong

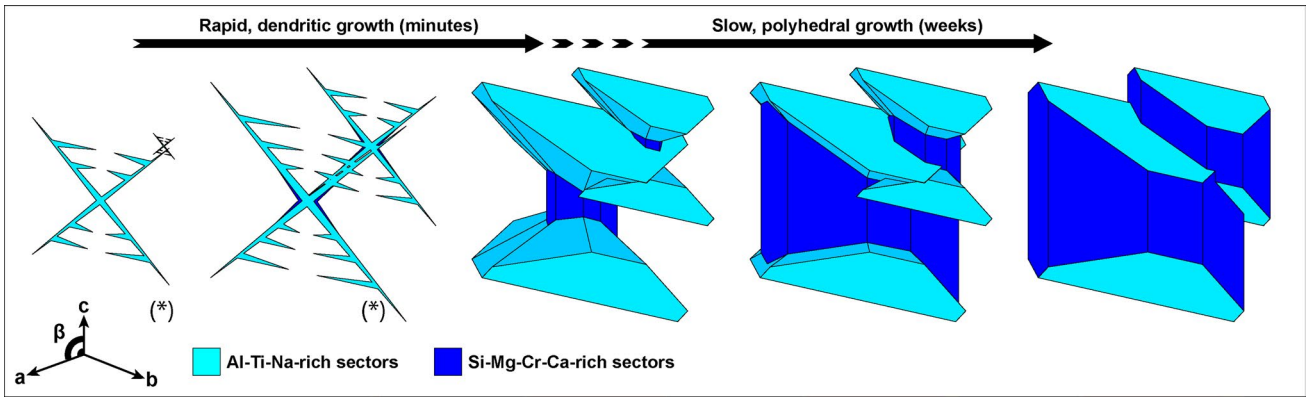

Fig. 13 Interpretative growth history of clinopyroxene phenocrysts in Qkuls ankaramite. Growth rates measurements (Kouchi et al. 1983) and qualitative observations of hollow crystals (Leung 1974; Rosenbusch 1888; Strong 1969; Wass 1973) suggest that rapid crystal growth was initiated by the development of fast-growing sectors {−111} (~10^{-6} m/s), followed by the development of slower-growing sectors {100}, {010} and {110} (10^{-7}–10^{-9} m/s). The growth rates of all sectors diminished down to 10^{-9} m/s as the degree of supersaturation decreased in the magma (from $-\Delta T > 25$ °C to $-\Delta T < 13$ °C), yielding to the maturation and infilling of skeletal and dendritic cavities. Because clinopyroxene was switching its growth mechanisms at that time (transitioning from diffusion-controlled to interface-controlled growth), it is probable that the sectors grew with a different composition during this second step of crystallization, hence the chemical heterogeneities within the sectors (Fig. 7). The crystal morphology of skeletal and dendritic clinopyroxene is simplified in the first two steps of growth [marked (*asterisk*)] since their actual geometries remains unknown at this date

1969). Differential, evolving values of growth rate and changing growth mechanisms of adjacent faces can produce parabolic or hyperbolic sector boundary surfaces (Gray 1971), which is consistent with the rounded contours of sectors in our clinopyroxene (Figs. 5, 6, 7, SM1 and 2). The fact that the spongy and nonspongy sectors are contiguous at the edges of crystals and are both in contact with the mesostasis (Figs. 5, 6, 7a, d) is consistent with an origin related to crystal growth.

In concentric zoning, compositional variation occurs radially to the crystal's core in response to time-varying environmental conditions or melt composition (e.g., Pearce 1984; Streck 2008). Sector zoning, in contrast, requires faces of the same crystal to be growing in a shared temperature, pressure and melt environment, yet incorporating elements in differing concentrations and producing an anisotropy of element partitioning among prominent crystal faces. Several theoretical models posit that the compositions of sectors are dictated primarily by the structure of the lattice exposed by the crystals faces (Dowty 1976; Hollister and Hargraves 1970; Larsen 1981; Nakamura 1973; Schwandt and McKay 2006; Shearer and Larsen 1994; Shimizu 1981; Skulski et al. 1994; Strong 1969; Watson and Liang 1995). Other models consider the additional effect of the diffusion rate of elements in the liquid when the growth rates exceed their mobility at the interface (Downes 1974; Kouchi et al. 1983; Larsen 1981; Leung 1974; Lofgren et al. 2006; McKay et al. 1986; Schwandt and McKay 2006; Strong 1969; Watson 1996). Although the origin of sector zoning is beyond the scope of this study, it is important to note that the sectors formed from a single melt, under ambient conditions of temperature and pressure, yet segregated the elements Al and Na that are considered to be pressure sensitive (Kornprobst et al. 1981; Putirka 2008; Thompson 1974) among different sectors. This has implications for clinopyroxene-based thermobarometry, as discussed in a companion article (Hammer et al. this issue). Given their geometrical and chemical complementarity, it is likely that both solid and spongy sectors of clinopyroxene phenocrysts interiors crystallized at identical, moderate pressures in the system. However, the depletion in Na of the outermost rims of all sectors suggests the reversal in domain distribution among sectors occurred after the crystals reached low pressure (Kornprobst et al. 1981; Thompson 1974), possibly during eruption and emplacement of the magma as a lava flow.

The intriguing behavior of Cr in the system deserves consideration. As a highly compatible element in clinopyroxene (Arth 1976), an uptick in the Cr concentration can be attributed to replenishment of the reservoir with more mafic basalt magma (e.g., Streck et al. 2002). It is possible that the increase in clinopyroxene Cr concentration toward crystal edges, particularly within spongy domains, is the result of magma mixing. A replenishment event may have mobilized the ankaramite magma to erupt, as has been suggested in other volcanic environments (Sinton and Detrick 1992). However, this first hypothesis is inconsistent with the absence of Mg enrichment in the outermost rims of clinopyroxene phenocrysts. Alternatively, a pseudo-open-system process producing the same pattern could be produced if crystals forming in a mushy region of the reservoir were liberated into a differentiated melt-rich part of

the reservoir, perhaps in association with volatile saturation and magma pressurization. This is a second scenario in which Cr enrichment in clinopyroxene could be associated with pre-eruptive magma mobilization in a compartmented reservoir. However, in light of evident kinetic controls on crystal growth, the Cr uptick does not require an open-system process. For example, the Cr enrichments and the presence of spinel inclusions in clinopyroxene may result from local enrichment in relatively slow-diffusing Cr and Al, and even in situ saturation of spinel within a compositional boundary layer surrounding rapidly growing clinopyroxene (Bacon 1989; Welsch et al. 2013).

Because melts have a unique composition at isothermal equilibrium, only one clinopyroxene composition can be in equilibrium with the melt. Thus, sector zoning indicates chemical disequilibrium during crystal growth. Compositional variations induce a difference in chemical potential of elements that drives homogenization by diffusion, and prolonged subsolidus diffusion should produce chemically homogeneous crystals. However, the mobility of elements is relatively slow in clinopyroxene (Cherniak and Dimanov 2010; Cherniak and Liang 2012), allowing compositional zoning to persist as a record of evolving growth environments.

Finally, the generally preserved growth faces of phenocrysts indicate that collision and breakage of crystals were limited in the conduit and in the reservoir. This is also consistent with the fresh aspect of the parting plane (100) in the mesostasis-free crystals, which indicates that fracture occurred during weathering out of the lava flow and not during transport in the magma conduit.

Implications for postshield reservoirs

Magma chambers presumably cool slowly, and the long-standing inference of slow cooling is production of euhedral minerals in conditions near equilibrium. However, our evidence of rapid growth for both clinopyroxene and olivine phenocrysts indicates that postshield magmas can achieve large degrees of supersaturation in deep-seated magma reservoirs. Rapid, diffusion-limited growth is possible at low cooling rates if (1) nucleation is delayed, e.g., if the magma is overheated or after an episode of magma recharge and overheating (Donaldson 1979; Faure et al. 2012), or (2) crystallization occurs within a diffusion field, such as the thermal and/or chemical gradients developed at the reservoir's margins. In the second case, the thermal gradient would likely be weak (<20 °C/cm, cooling rate <5 °C/h; Donaldson 1977; Faure et al. 2006; Bouquain et al. 2014), since, except for twins {100}, the crystals do not show a marked elongation along a particular crystallographic axis. These situations may happen during a recharge, when a fresh magma is transported in the cold margins of a crustal reservoir. Clinopyroxene co-crystallizes then with olivine, forming a mush of maturing dendrites. As the magma crystallizes these minerals, the concentration of volatiles increases in the remaining liquid. The exsolution of volatiles, as indicated by the presence of vesicles within the spongy sectors {hk0} of clinopyroxene phenocrysts, would pressurize the reservoir, eventually enough to create fractures and extract the ankaramitic mush toward the surface.

Conclusions

This study shows that sector zoning can be used to probe magmatic clinopyroxene growth environments. The ubiquity of parallel crystal growth units and defects, including melt-filled cavities, twins, and subgrain angular misorientations, all indicate that clinopyroxene phenocrysts in the ankaramite experienced initial rapid growth prior to eruption. Compositional zoning patterns are consistent with sector zoning type of the type $(Al + Ti)_{\{-111\}} = (Si + Mg)_{\{hk0\}}$, and also indicate rapid growth at a high degree of undercooling ($-\Delta T = 45$ °C). After the first burst of crystallization, clinopyroxene subsequently grew in conditions approaching equilibrium, developing external flat faces on the top of the hourglass structure. This is marked in the sectors by partial infilling with clinopyroxene of new composition. Finally, a reversal in the distribution of both textures and element partitioning with respect to zones very late in crystal growth history indicates that the ankaramite crystals completed growth near or at the surface at low degree of supersaturation. This evolving crystal growth contradicts the inferences that minerals in deep-seated reservoirs grow slowly near equilibrium, and the assumption that crystal growth is fastest at near-surface or syn-emplacement conditions.

Acknowledgments We thank Keith Putirka and Matteo Masotta for detailed comments on the first version of the manuscript. We are grateful to JoAnn Sinton and Emily First for providing samples, and to Thomas Shea for collecting some of the X-ray maps. JoAnn Sinton is also thanked for the preparation of the thin sections. This work was supported by NSF EAR 12-20084 to JEH. This is School of Ocean and Earth Sciences and Technologies (SOEST; University of Hawaii) contribution 9530.

References

Arth JG (1976) Behavior of trace elements during magmatic processes: a summary of theoretical models and their applications. J Res US Geol Surv 4(1):41–47

Bacon CR (1989) Crystallization of accessory phases in magmas by local saturation adjacent to phenocrysts. Geochim Cosmochim Acta 53(5):1055–1066

Bouquain S, Arndt NT, Faure F, Libourel G (2014) An experimental study of pyroxene crystallization during rapid cooling

in a thermal gradient: application to komatiites. Solid Earth 5(2):641–650. doi:10.5194/se-5-641-2014
Brugger CR, Hammer JE (2015) Prevalence of growth twins among anhedral plagioclase microlites. Am Miner 100(2–3):385–395. doi:10.2138/am-2015-4809
Buerger MJ (1932) The significance of block structure in crystals. Am Mineral 17:177–191
Buerger MJ (1934) The lineage structure of crystals. Z Kristallogr Miner 89:195–220
Buerger MJ (1945) The genesis of twin crystals. Am Miner 30:469–482
Cameron M, Papike JJ (1981) Structural and chemical variations in pyroxenes. Am Miner 66:1–50
Chalmers B (1964) Principles of solidification. Wiley, New York
Chatterjee N, Bhattacharji S, Fein C (2005) Depth of alkalic magma reservoirs below Kolekole cinder cone, Southwest rift zone, East Maui, Hawaii. J Volcanol Geotherm Res 145(1–2):1–22. doi:10.1016/j.jvolgeores.2005.01.001
Cherniak DJ, Dimanov A (2010) Diffusion in pyroxene, mica and amphibole. Rev Miner Geochem 72(1):641–690
Cherniak DJ, Liang Y (2012) Ti diffusion in natural pyroxene. Geochim Cosmochim Acta 98:31–47. doi:10.1016/j.gca.2012.09.021
Clark JR, Appleman DE, Papike JJ (1969) Crystal-chemical characterization of clinopyroxenes based on eight new structure refinements. Miner Soc Am Spec Pap 2:31–50
Corrigan GM (1982) Supercooling and the crystallization of plagioclase, olivine, and clinopyroxene from basaltic magmas. Miner Mag 46(March):31–42
Cross W (1915) Lavas of Hawaii and their relations. Government Printing Office, Washington
Daly RA (1911) Magmatic differentiation in Hawaii. J Geol 19(4):289–316
Deer WA (1997) Rock-forming minerals, 2nd edn. Geol. Soc, London
Donaldson CH (1977) Laboratory duplication of comb layering in the Rhum pluton. Miner Mag 41(September):323–336
Donaldson CH (1979) An experimental investigation of the delay in nucleation of olivine in mafic magmas. Contrib Miner Pet 69(1):21–32
Downes MJ (1974) Sector and oscillatory zoning in calcic augites from M. Etna, Sicily. Contrib Miner Pet 47(3):187–196. doi:10.1007/bf00371538
Dowty E (1976) Crystal structure and crystal growth. II. Sector zoning in minerals. Am Miner 61(5–6):460–469
Dowty E (1977) The importance of adsorption in igneous partitioning of trace elements. Geochim Cosmochim Acta 41(11):1643–1646
Dowty E (1980) Computing and drawing crystal shapes. Am Miner 65(5–6):465–471
Dowty E (1987) SHAPE Copyright 1994, Shape Software 521 Hidden Valley Road, Kingsport, TN 37663 USA. http://www.shapesoftware.com
Duncan AM, Preston RMF (1980) Chemical variation of clinopyroxene phenocrysts from the trachybasaltic lavas of Mount Etna, Sicily. Miner Mag 43:765–770
Faquhar OC (1960) Occurrences and origin of the hourglass structure. Rep 21st Sess Int Geol Congr, Norden 21:194–200
Faure F, Tissandier L (2014) Contrasted liquid lines of descent revealed by olivine-hosted melt inclusions and the external magma. J Petrol 55(9):1779–1798
Faure F, Trolliard G, Nicollet C, Montel J-M (2003a) A developmental model of olivine morphology as a function of the cooling rate and the degree of undercooling. Contrib Miner Pet 145(2):251–263
Faure F, Trolliard G, Soulestin B (2003b) TEM investigation of forsterite dendrites. Am Miner 88(8–9):1241–1250
Faure F, Arndt N, Libourel G (2006) Formation of spinifex texture in komatiites: an experimental study. J Petrol 47(8):1591–1610
Faure F, Schiano P, Trolliard G, Nicollet C, Soulestin B (2007) Textural evolution of polyhedral olivine experiencing rapid cooling rates. Contrib Miner Pet 153(4):405–416
Faure F, Tissandier L, Libourel G, Mathieu R, Welsch B (2012) Origin of glass inclusions hosted in magnesian porphyritic olivines chondrules: deciphering planetesimal compositions. Earth Planet Sci Lett 319–320:1–8. doi:10.1016/j.epsl.2011.12.013
Ferguson AK (1973) On hour-glass sector zoning in clinopyroxene. Miner Mag 39:321–325
Fodor RV, Keil K, Bunch TE (1975) Contributions to the mineral chemistry of Hawaiian rocks. IV. Pyroxenes in rocks from Haleakala and West Maui volcanoes, Maui, Hawaii. Contrib Miner Pet 50(3):173–195. doi:10.1007/bf00371038
Gray NH (1971) A parabolic hourglass structure in titanaugite. Am Miner 56:952–958
Hammer JE, Jacob S, Welsch B, Hellebrand E, Sinton J (this issue) Clinopyroxene in postshield Haleakala ankaramite. 1. Efficacy of thermobarometry. Contrib Mineral Petrol. doi:10.1007/s00410-015-1212-x
Hartman P, Perdok WG (1955a) On the relations between structure and morphology of crystals. Acta Crystallogr 8:49–52
Hartman P, Perdok WG (1955b) On the relations between structure and morphology of crystals. Acta Crystallogr 8:521–524
Hartman P, Perdok WG (1955c) On the relations between structure and morphology of crystals. Acta Crystallogr 8:525–529
Helz RT (1987) Diverse olivine types in lava of the 1959 eruption of Kilauea volcano and their bearing on eruption dynamics. US Geol Surv Prof Pap 1350:691–722
Herring C (1951) Some theorems on the free energies of crystal surfaces. Phys Rev 82(1):87–93
Hollister LS, Gancarz AJ (1971) Compositional sector zoning in clinopyroxene from the Narce area, Italy. Am Miner 56:950–979
Hollister LS, Hargraves RB (1970) Compositional zoning and its significance in pyroxenes from two coarse grained Apollo 11 samples. In: Proceedings of Apollo 11 lunar science conference, vol 1, pp 541–550
Kirkpatrick RJ (1975) Crystal growth from the melt: a review. Am Miner 60:798–814
Kornprobst J, Ohnenstetter D, Ohnenstetter M (1981) Na and Cr contents in clinopyroxenes from peridotites: a possible discriminant between "sub-continental" and "sub-oceanic" mantle. Earth Planet Sci Lett 53(2):241–254
Kouchi A, Sugawara Y, Kashima K, Sunagawa I (1983) Laboratory growth of sector zoned clinopyroxenes in the system CaMgSi2O6–CaTiAl2O6. Contrib Miner Pet 83(1):177–184
Kretz R (1983) Symbols for rock-forming minerals. Am Miner 68:277–279
Kuo L-C, Kirkpatrick RJ (1982) Pre-eruption history of phyric basalts from DSDP Legs 45 and 46: evidence from morphology and zoning patterns in plagioclase. Contrib Miner Pet 79:13–27
Kuo L-C, Kirkpatrick RJ (1985) Kinetics of crystal dissolution in the system diopside-forsterite-silica. Am J Sci 285(1):51–90
Larsen LM (1981) Sector zoned aegirine from the Ilímaussaq alkaline intrusion, South Greenland. Contrib Miner Pet 76(3):285–291. doi:10.1007/bf00375455
Leung IS (1974) Sector-zoned titanaugites: morphology, crystal chemistry, and growth. Am Miner 59(1–2):127–138
Lofgren GE, Donaldson CH (1975) Curved branching crystals and differentiation in comb-layered rocks. Contrib Miner Pet 49(4):309–319. doi:10.1007/bf00376183
Lofgren GE, Huss GR, Wasserburg GJ (2006) An experimental study of trace-element partitioning between Ti–Al-clinopyroxene and melt: equilibrium and kinetic effects including sector zoning. Am Miner 91(10):1596–1606
McKay G, Wagstaff J, Yang SR (1986) Clinopyroxene REE distribution coefficients for shergottites: the REE content of the

Shergotty melt. Geochim Cosmochim Acta 50(6):927–937. doi:10.1016/0016-7037(86)90374-1
Milman-Barris M, Beckett J, Baker M, Hofmann A, Morgan Z, Crowley M, Vielzeuf D, Stolper E (2008) Zoning of phosphorus in igneous olivine. Contrib Miner Pet 155(6):739–765
Nakamura Y (1973) Origin of sector zoning of igneous clinopyroxenes. Am Miner 58:986–990
Ni H, Keppler H, Walte N, Schiavi F, Chen Y, Masotta M, Li Z (2014) In situ observation of crystal growth in a basalt melt and the development of crystal size distribution in igneous rocks. Contrib Miner Pet 167(5):1–13. doi:10.1007/s00410-014-1003-9
Pearce TH (1984) The analysis of zoning in magmatic crystals with emphasis on olivine. Contrib Miner Pet 86(2):149–154. doi:10.1007/bf00381841
Putirka KD (2008) Thermometers and barometers for volcanic systems. Rev Miner Geochem 69(1):61–120
Romé de l'Isle J-B (1783) Cristallographie, ou description de formes propres à tous les corps du règne minéral. Imprimerie de Monsieur, Paris
Rosenbusch H (1888) Microscopical physiography of the rock-making minerals: An aid to the microscopical study of rocks. Wiley, New York
Schwandt CS, McKay GA (2006) Minor- and trace-element sector zoning in synthetic enstatite. Am Miner 91(10):1607–1615
Schwindinger KR (1999) Particle dynamics and aggregation of crystals in a magma chamber with application to Kilauea Iki olivines. J Volcanol Geotherm Res 88(4):209–238
Schwindinger KR, Anderson AT (1989) Synneusis of Kilauea Iki olivines. Contrib Miner Pet 103(2):187–198
Shearer CK, Larsen LM (1994) Sector-zoned aegirine from the Ilímaussaq alkaline intrusion, South Greenland: implications for trace element behavior in pyroxene. Am Miner 79:340–352
Shimizu N (1981) Trace element incorporation into growing augite phenocryst. Nature 289(5798):575–577
Sinton JM, Detrick RS (1992) Mid-ocean ridge magma chambers. J Geophys Res 97(B1):197–216. doi:10.1029/91JB02508
Skulski T, Minarik W, Watson EB (1994) High-pressure experimental trace-element partitioning between clinopyroxene and basaltic melts. Chem Geol 117(1–4):127–147. doi:10.1016/0009-2541(94)90125-2
Stearns HT, Macdonald GA (1942) Geology and ground-water resources of the island of Maui, Hawaii. Hawaii Div Hydrography Bull 7344
Steno N (1669) De Solido Intra Sodium Naturaliter Contento Dissertations Prodomus. Florence, English translation by JG Winter The Prodomus of Nicolaus Steno's Dissertation Concerning a Solid Body Enclosed by Process of Nature Within a Solid, Hafner, New York 1968
Streck MJ (2008) Mineral textures and zoning as evidence for open system processes. Rev Miner Geochem 69(1):595–622
Streck M, Dungan M, Malavassi E, Reagan M, Bussy F (2002) The role of basalt replenishment in the generation of basaltic andesites of the ongoing activity at Arenal volcano, Costa Rica: evidence from clinopyroxene and spinel. Bull Volcanol 64(5):316–327. doi:10.1007/s00445-002-0209-2
Streck MJ, Dungan MA, Bussy F, Malavassi E (2005) Mineral inventory of continuously erupting basaltic andesites at Arenal volcano, Costa Rica: implications for interpreting monotonous, crystal-rich, mafic arc stratigraphies. J Volcanol Geotherm Res 140(1–3):133–155. doi:10.1016/j.jvolgeores.2004.07.018
Strong DF (1969) Formation of the hour-glass structure in augite. Miner Mag 37(288):472–479
Stull RJ (1979) Mantled feldspars and synneusis. Am Miner 64:514–518
Sunagawa I (1981) Characteristics of crystal growth in nature as seen from the morphology of mineral crystals. Bull Miner 104:81–87
Sunagawa I (2005) Crystals: growth, morphology and perfection. Cambridge University Press, Cambridge
Thompson RN (1974) Some high-pressure pyroxenes. Miner Mag 39(September):768–787
Wadsworth WJ (1961) The layered ultrabasic rocks of South-West Rhum, Inner Hebrides. Philos Trans R Soc Lond B 244(707):21–64
Washington S, Mervin HE (1922) Augite of Haleakala, Maui, Hawaiian Islands. Am J Sci 5th series 3(14):117–122
Wass SY (1973) The origin and petrogenetic significance of hour-glass zoning in titaniferous clinopyroxenes. Miner Mag 39(302):133–144. doi:10.1180/minmag.1973.039.302.01
Watson EB (1996) Surface enrichment and trace-element uptake during crystal growth. Geochim Cosmochim Acta 60(24):5013–5020
Watson EB, Liang Y (1995) A simple model for sector zoning in slowly grown crystals: implications for growth rate and lattice diffusion, with emphasis on accessory minerals in crustal rocks. Am Miner 80:1179–1187
Welsch B, Faure F, Famin V, Baronnet A, Bachèlery P (2013) Dendritic crystallization: a single process for all the textures of olivine in basalts? J Petrol 54(3):539–574
Welsch B, Hammer JE, Hellebrand E (2014) Phosphorus reveals dendritic architecture of olivine. Geology 42(10):867–870. doi:10.1130/G35691.1